International Journal of Solids and Structures 46 (2009) 2493–2505

Contents lists available at ScienceDirect

International Journal of Solids and Structures

journal homepage: www.elsevier.com/locate/ijsolstr

Experimental and numerical studies of creasing of paperboard

Mikael Nygårds [a,*], Magnus Just [b], Johan Tryding [b]

[a] STFI-Packforsk AB, Box 5604, SE-114 86 Stockholm, Sweden
[b] Tetra Pak Packaging Solutions AB, Ruben Rausings gata, SE-221 86 Lund, Sweden

ARTICLE INFO

Article history:
Received 23 October 2008
Received in revised form 28 January 2009
Available online 3 March 2009

Keywords:
Creasing
Paperboard
Experiment
Elastic
Plastic
Finite element method

ABSTRACT

A laboratory creasing device to capture the most important properties of a commercial rotary creasing tool was designed. Finite element analysis of the creasing of a multiply paperboard in the laboratory crease device was presented. The multiply paperboard was modeled as a multilayered structure with cohesive softening interface model connecting the paperboard plies. The paperboard plies were modeled by an anisotropic elastic–plastic material model. The purpose of the analysis of the laboratory creasing device was to present material models that represent paperboard, and to investigate how well the analysis captured the multiply paperboard behavior during laboratory creasing. And to increase the understanding of what multiply paperboard properties that influence the laboratory crease operation. The result of the simulations showed very good correlations with the experimental obtained results. The results indicated that the paperboard properties that have the most influence is the out-of-plane shear, out-of-plane compression and the friction between the laboratory creasing device and the paperboard.

1. Introduction

Paper consists of a network of bonded fibers that is formed by draining a fiber suspension through a filter screen. Paperboard is a paper material that often consists of several plies, especially if it is used in creasing operations. The different plies are bonded chemically to each other either by starch or other adhesive materials. In Fig. 1 the cross section of a paperboard can be seen. It can be observed that the outer plies, that are roughly 0.1 mm thick, have higher density than the middle ply.

The creasing operation in a commercial converting plant utilize the fact that the paperboards have very different in-plane and out-of-plane properties to achieve a permanent, smooth and good enough fold notch that enable forming and folding to a given geometry without surface cracking, cf. Hine (1987), Cavlin (1988), Cavlin et al. (1997), Nagasawa et al. (2003, 2008). The operation introduces local damage in the out-of-plane paperboard properties in order to create better and more well-defined folding lines during the subsequent folding (Hine, 1987). It is mainly shear deformations that cause the material to delaminate during the creasing operation, cf. Hine (1987), Dunn (2000). The existing knowledge about the process is mainly based on empirical studies, and the damage mechanisms are not well understood. Apart from the observed delamination deformation it has not been possible to identify the different tensile, compressive and shear strain components, nor has the delamination displacement been quantified in paper materials. This is a typical process where modeling and simulation would contribute positively to the understanding of the damage process in the material.

In the literature Carlsson et al. (1982) have used the finite element method to study creasing. At these initial studies the J-integral was used. Experimental studies with created delamination sites have also been conducted, where it has been shown that the creasing and bending behavior depends greatly on the delamination behavior (Carlsson et al., 1983).

To enable numerical studies of damage and deformation in paperboard, material models that mimic paper materials must be used. Generally this is a problem since paper materials due to the fibrous structure are extremely anisotropic, when both the in-plane and out-of-plane directions shall be accounted for. The stiffness in the machine direction (hereinafter labeled MD or x) can be 1–5 times higher than the stiffness in the cross-machine direction (hereinafter labeled CD or y), and 100 times higher than the stiffness in the out-of-plane direction (hereinafter labeled ZD or z) (Baum et al., 1981; Stenberg, 2002a). The anisotropy can result in numerical problems when material models are numerically implemented. Therefore, in continuum modeling of paper materials the assumption that the out-of-plane Poisson's ratio is zero,

$$\nu_{xz} = \nu_{yz} = \nu_{zx} = \nu_{zy} = 0 \tag{1}$$

can be utilized (Xia, 2002). Experimental data also support that the out-of-plane Poisson's ratio is close to zero (Öhrn, 1965; Stenberg and Fellers, 2002). In the elastic regime Hooke's generalized law can be used to show that the in-plane and out-of-plane models will be uncoupled with the assumption of Eq. (1). If the assumption also

* Corresponding author. Tel.: +46 86767193; fax: +46 84115518.
E-mail address: mikael.nygards@stfi.se (M. Nygårds).

0020-7683/$ - see front matter © 2009 Elsevier Ltd. All rights reserved.
doi:10.1016/j.ijsolstr.2009.02.014

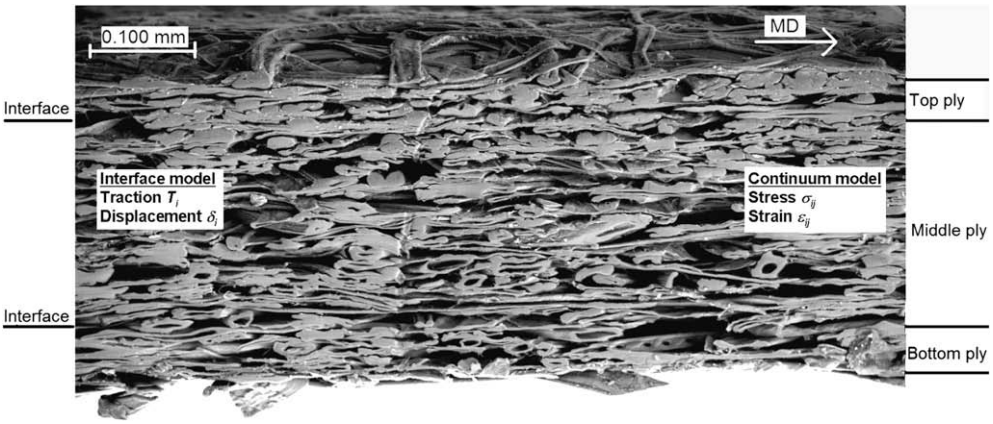

Fig. 1. SEM picture of the paperboard cross section. Note, the picture was taken in a vacuum chamber, therefore the thickness has been decreased. In the modeling approach the paperboard was represented by a combination of continuum and interface models.

holds for the plastic regime, the in-plane and out-of-plane models can be solved separately, which is preferred from a numerical point of view.

For the in-plane behavior of paper materials there are in-plane models that describe the MD and CD directions well, see e.g. Trydding (1996) and Mäkelä and Östlund (2003). Biaxial data is however rare in the literature, one of only a few references available in the literature is deRuvo et al. (1980). A model that is based on the data by deRuvo et al. (1980) is the elastic–plastic in-plane continuum model proposed by Xia et al. (2002). An anisotropic yield surface with non-linear hardening functions is used, where plasticity was initiated by a yield surface constructed from"yield planes" for tension and compression in MD and CD as well as shear. The drawback with the model is that it is difficult to calibrate correctly the model parameters. Another yield surface based on the Tsai-Wu criteria was proposed by Harrysson (2007). This model is based on biaxial testing of liner and fluting. Harrysson (2007) addressed many of the difficulties with large deformations and anisotropy. Based on these findings Ask (2007) implemented a modified version of the in-plane model proposed by Xia et al. (2002).

To account for deformation and damage in paperboard a successful combination of continuum and cohesive models have been used by Xia (2002). Xia (2002) used a continuum model expressed in stresses and strains to represent each ply. To represent the interfaces between the plies cohesive elements, where the constitutive equations were expressed by tractions and displacements, were utilized. This modeling concept is schematically shown on top of the microstructure photo in Fig. 1. However, the continuum in-plane model proposed by Xia et al. (2002) only had an elastic out-of-plane model. It was assumed that continuum plasticity in the out-of-plane direction was of less importance, since the model should be used together with a interface model that would account for damage in the out-of-plane directions. This model has been implemented by Nygårds et al. (2005), to study and experimentally verify the creasing and folding operations. It was found that the elastic out-of-plane model did not capture the experimental creasing behavior during unloading.

In multiply paperboards the different plies are bonded chemically, hence no fibers cross the interfaces. Normally interfaces introduce weaker regions in the thickness direction, which are essential to maintain good convertability of paperboard. Due to the paperboard design, delamination between plies is a dominating damage mechanism, which for folding has been experimentally verified by Dunn (2000). In order to account for delamination in paperboards Xia (2002) proposed a cohesive interface model. The model is elastic–plastic with plastic softening with respect to strength and stiffness. Xia (2002) used the interface model implemented as an cohesive element together with a continuum model for simulation of creasing and subsequent folding of paperboard. Hallbäck et al. (2006) used a similar interface formulation to study delamination in printing applications. In this work a CD crease, where the crease line run in the CD direction will be investigated. For this configuration experimental and numerical studies will be presented.

2. Experimental creasing setup

In Fig. 2, a 3D-CAD drawing of the laboratory creasing tool setup is shown. The creasing tool unit was mounted into a MTS 858 Table Top System with a force capacity of 25 kN. The MTS 858 Table Top piston was fixed to the creasing tools male die holder and the creasing tool bottom plate was fixed to the MTS 858 Table Top bottom plate. To allow for exchangeability of different male die geometries the male die was mounted in a holder. The male die holder movement was restricted to ZD-directional movement by rails mounted on the U-bolt shown in Fig. 2. The female die was mounted on the 15 kN axial load cell (MTS model 661.19F-03) and the load cell was mounted on the MTS 858 Table Top.

A schematic 2D-sketch in the *xz*-plane of the creasing tool in Fig. 2 is shown in Fig. 3. The upper and lower tools in the figure are the male die and the female die, respectively. The male die tool in Fig. 3 has a ruler that stick out from the base, where the ruler width was 0.9 mm. The height of the ruler used was 0.8 mm, with a flat ruler tip. At creasing, the paperboard between the tools was

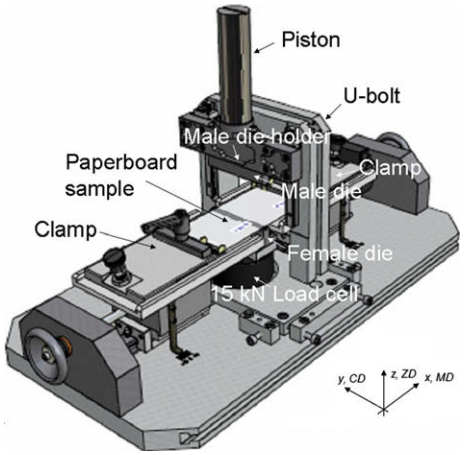

Fig. 2. A 3D-CAD sketch of the laboratory creasing tool setup unit. The base plate dimensions was 750 × 390 mm and the hight of the U-bolt from the base was 280 mm.

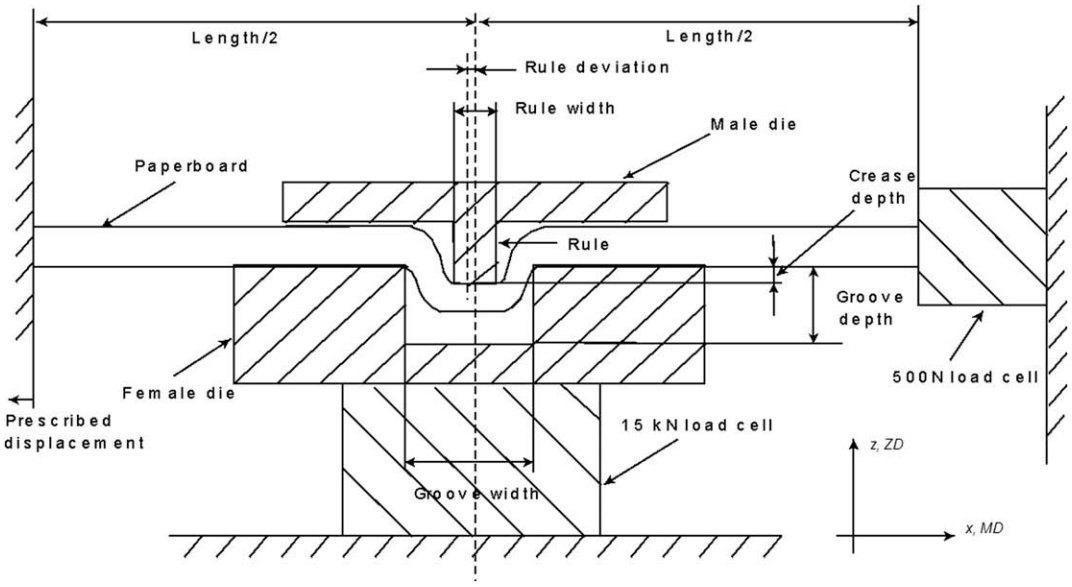

Fig. 3. A principle 2 D-sketch of the creasing tool with load cells and boundary conditions for the mounted paperboard sample.

pressed into a groove in the female die tool. The width of the groove in the tests was 1.6 mm and the depth of the groove was 0.8 mm. The male and female tools alignment was set by the rule deviation, see Fig. 3. The rule deviation was adjusted to be 0.00 mm. In the set up the female die plate had hight 21 mm, width 14 mm and length 110 mm.

The paperboard sample had length 110 mm and width 38 mm. The MD-direction of the paperboard was parallel to the *x*-direction in Fig. 2. The sample was symmetrically positioned between the crease tools, and was clamped at each side, as seen in Figs. 2 and 3. The length between the clamps was 80 mm. The paperboard was given a prescribed displacement until the 500 N load cell display a web tension of 1.0 kN/m. The 500 N axial load cell (MTS model 661.11B-02) was mounted on the creasing tool, see Fig. 3.

During the creasing operation the ruler press the paperboard into the groove, as seen in Fig. 3. The force in the ZD-direction (crease force) and the MD-direction (in-plane force) was during the operation measured by the 15 kN and the 500 N axial load cell, respectively. The speed of the rule was set to 1.0 mm/s. The distance the rule travel was monitored by a displacement gage (MTS model 632.06H-30 OPT 002) that was mounted on the U-bolt. The relative distance between the male and female tools was denoted crease depth. The crease depths used were 0.0 mm and 0.2 mm.

The tests were made at a relative humidity of 50 ± 2% and at a temperature of 23 ± 1 °C.

3. Finite element model

ABAQUS (2008) have developed a cohesive element that will be used to represent the interface model. By this approach the whole paperboard will be represented by elements, instead of a using a contact formulation to represent the interface. This could have been an alternative, which could have been done by using the UINTER interface (ABAQUS, 2008).

3.1. Parts and mesh

The finite element model has been created in ABAQUS/CAE (ABAQUS, 2008). In Fig. 4 the whole assembly representing paperboard and the creasing tools can be seen. To mimic the experimental setup a male die with width 0.90 mm, with sharp edges, was used. The female die had width 1.6 mm, where the edges were rounded with circular segments with radius 0.2 mm. This prevented penetration of the female die edge into the paperboard, which improved the convergence of the finite element model.

3.2. Continuum model

In order to simplify the numerical implementation of the continuum model we assume that the out-of-plane Poisson's ratio is zero, according to Eq. (1). Hence, the in-plane and out-of-plane models were assumed to be uncoupled, and therefore solved independently. Stenberg and Fellers (2002) have shown that the out-of-plane Poisson's ratio is zero or negative for different paper qualities. They also showed that there are no difference between the elastic and plastic regimes. This observation should justify the approximation of zero Poisson's ratio. When realistic material properties for paperboard have been used several numerical problems due to the anisotropic behavior have been identified. The model we propose here is the one that work best within the given premises. As a consequence of this the out-of-plane problem was solved by the utilization of one yield surface in compression and one in shear, where the model has a coupling between compressive and shear stresses in the out-of-plane shear hardening modulus.

3.2.1. In-plane model

The elastic–plastic in-plane model assumes linear elasticity and utilizes a plasticity model that has been proposed by Xia et al. (2002), which in a modified version has been implemented by Andersson (2006). The yield criterion was constructed by six yield planes, which represent yielding in: MD tension, CD tension, positive shear, MD compression, CD compression and negative shear. In the in-plane model plastic deformation occurs when the yield surface, $f^{in-plane}$, is zero,

$$f^{in-plane} = \sum_{I=1}^{6} \chi_I \left(\frac{\boldsymbol{\sigma} : \boldsymbol{N}_I}{\sigma_s^I} \right)^{2k} - 1 = 0, \tag{2}$$

where $\boldsymbol{\sigma}$ is the in-plane stress tensor, σ_s^I is the yield stress and $\boldsymbol{N}_I$ is the normal direction of the yield planes and k is a positive integer. More details about the yield criteria and determination of parame-

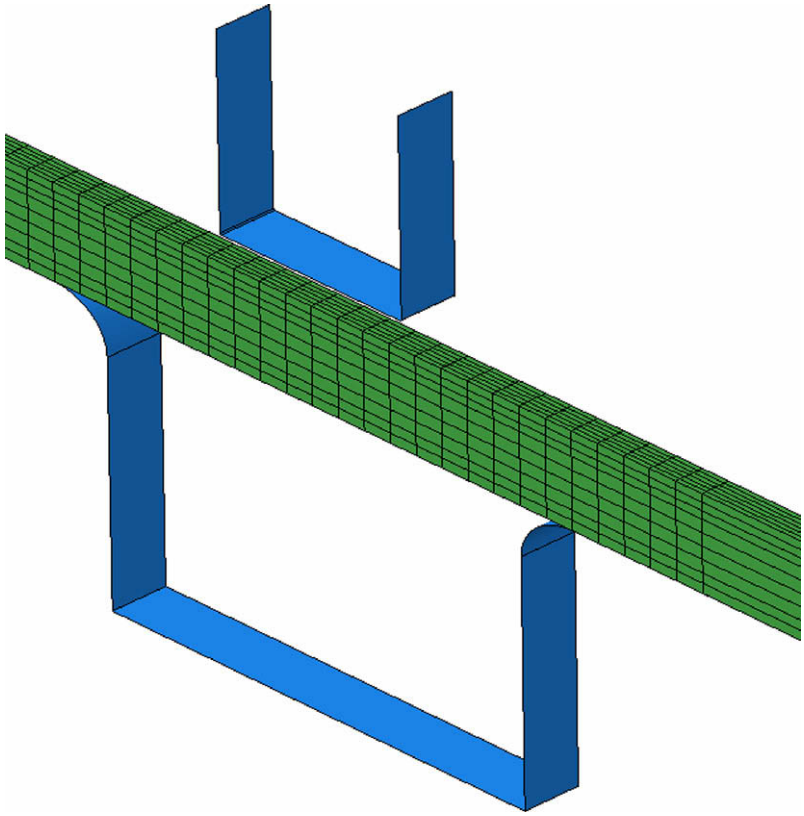

Fig. 4. The paperboard, female die and male rule assembly in the crease area.

ters are found in Xia et al. (2002) or alternatively in Ask (2007). The switching parameter χ_I was defined as

$$\chi_I = \begin{cases} 1 & \text{if } \boldsymbol{\sigma} : \boldsymbol{N}_I > 0; \\ 0 & \text{otherwise.} \end{cases} \tag{3}$$

In the model associated plastic flow was assumed, and the hardening for the different yield planes was expressed as

$$\sigma_s^I = \sigma_{s0}^I + A^I tanh(B^I \varepsilon_{eff}^p) + C^I \varepsilon_{eff}^p \tag{4}$$

$$\sigma_s^{II} = \sigma_{s0}^{II} + A^{II} tanh(B^{II} \varepsilon_{eff}^p) + C^{II} \varepsilon_{eff}^p \tag{5}$$

$$\sigma_s^{III} = \sigma_{s0}^{III} + A^{III} tanh(B^{III} \varepsilon_{eff}^p) + C^{III} \varepsilon_{eff}^p \tag{6}$$

$$\sigma_s^{IV} = \sigma_{s0}^{IV} + A^{IV} tanh(B^{IV} \varepsilon_{eff}^p) + C^{IV} \varepsilon_{eff}^p \tag{7}$$

$$\sigma_s^{V} = \sigma_{s0}^{V} + A^{V} tanh(B^{V} \varepsilon_{eff}^p) + C^{V} \varepsilon_{eff}^p \tag{8}$$

$$\sigma_s^{VI} = \sigma_s^{III}(\varepsilon_{eff}^p), \tag{9}$$

where σ_{s0}^i is the initial yield stress and A^i, B^i and C^i are the hardening parameters. The exponent i refers to the different yield planes where $i = I$ is MD tension, $i = II$ is MD compression, $i = III$ is positive shear, $i = IV$ is CD tension, $i = V$ is CD compression, while $i = VI$ is negative shear. The effective plastic strain, ε_{eff}^p was defined as

$$\varepsilon_{eff}^p = \sqrt{\left(\varepsilon_{xx}^p\right)^2 + \left(\varepsilon_{yy}^p\right)^2 + \left(\frac{\gamma_{xy}^p}{2}\right)^2}, \tag{10}$$

where ε_{xx}^p and ε_{yy}^p were the plastic strains in the x and y directions, and γ_{xy}^p was the plastic in-plane shear strain.

3.2.2. Out-of-plane model

The elastic part of the out-of-plane model was constructed to mimic experimental observations of paperboard in the out-of-plane direction. Paperboard that consists of a network structure of hollow fibers exhibit an exponential behavior when it is compressed. While it is linear in tension, at least until the onset of delamination (Nygårds, 2008). Therefore, the normal stress, σ_{zz}, was divided into separate compressive and tensile behaviors,

$$\sigma_{zz} = \begin{cases} E_z \varepsilon_{zz}^e & \text{if } \varepsilon_{zz}^e > 0 \\ E_c(1 - e^{-C_c \varepsilon_{zz}^e}) & \text{otherwise,} \end{cases} \tag{11}$$

where ε_{zz}^e was the elastic strain in the z-direction, E_z, E_c, C_c and G were elastic material constants.

At shear loading paperboard has been observed to be linear in the elastic regime, with no significant difference in the MD and CD directions (Nygårds, 2008). Therefore the shear stresses, τ_{xz} and τ_{yz}, were assumed to have the same shear modulus, G, hence

$$\tau_{xz} = G\gamma_{xz}, \tag{12}$$

$$\tau_{yz} = G\gamma_{yz}. \tag{13}$$

The linear elastic constants were determined from least square fits in initial part the of experimental stress-strain curves, while E_c and C_c were fitted to the unloading part of compression stress-strain curves.

The plastic behavior was divided into two parts. One yield surface for compression, f^{comp}, that was assumed to be uncoupled from the shear behavior. The model was assumed to be elastic–plastic in compression, while it was only elastic in tension. Instead the interface model will capture the inelastic behavior in tension. The yield surface for compression, f^{comp}, was expressed in term of the normal stress in the z-direction, σ_{zz}, and the yield stress in compression, σ_{zz}^s, hence plastic deformation was initiated when the yield criterion was equal to zero,

$$f^{comp} = -\sigma_{zz} - \sigma_{zz}^s = 0, \tag{14}$$

where

$$\sigma_{zz}^s = B_p\left(e^{C_p \varepsilon_{zz}^p} - 1\right), \tag{15}$$

where B_p and C_p are material constants that describe the plastic hardening. These were fitted to loading part of a compression stress-strain curve, from which the elastic behavior had been substracted.

From experimental data it has been observed that the hardening coefficient in shear increases when a compressive stress in the ZD direction is applied (Stenberg, 2002b). Therefore, a σ_{zz} component was incorporated in the shear yield stress, τ_s. The yield surface for shear, f^{shear}, was expressed in terms of shear stresses, τ_{xy} and τ_{yz}, and the shear yield stress, τ_s. Plastic deformation was initiated when the yield criterion was zero,

$$f^{shear} = \sqrt{\tau_{xy}^2 + \tau_{yz}^2} - \tau_s = 0, \tag{16}$$

where

$$\tau_s = \tau_0 + (A_\tau - \sigma_{zz} B_\tau)\gamma^p \tag{17}$$

and τ_0 was the initial yield in out-of-plane shear, A_τ was the hardening coefficient in shear in absence of delamination failure, and B_τ was a coupling constant between normal and shear stresses. It was difficult to perform a experimental test to determine A_τ and B_τ, therefore the loading part of a creasing curve was utilized, as described in the results section of the manuscript.

3.3. Cohesive model

The cohesive elements account for delamination in the paperboard. The constitutive equations used in this work were formulated by tractions and displacements. The model presented in this section follows the model proposed by Xia (2002), but the functions for the strength and stiffness degradation has been altered in order to better capture experimental observations. Moreover, only associated plastic flow was assumed. The model should be used together with a continuum model. In the cohesive model a local coordinate system with axes 1, 2 and 3 was used. The 1-direction was the interface normal direction, hence the out-of-plane (ZD) direction in the paperboard. The 2 and 3 directions corresponds to the orthogonal tangents to the interface, hence the machine (MD) and cross machine (CD) directions respectively in the paperboard. These are the principal directions for the orthotropic material behavior of paperboard.

The model proposed by Xia (2002) is an elastic–plastic cohesive model expressed in terms of tractions and displacements. The relative displacement between two opposing surfaces is divided into elastic and plastic parts. Each displacement component, δ_i, where $i = 1, 2, 3$, is divided into

$$\delta_i = \delta_i^e + \delta_i^p, \tag{18}$$

where δ_i^e is the elastic displacement and δ_i^p is the plastic displacement referred to the local coordinate system at the interface. The division into elastic and plastic displacements of the total displacement increment $\Delta\delta_i$ also holds during a time increment Δt, hence

$$\Delta\delta_i = \Delta\delta_i^e + \Delta\delta_i^p, \tag{19}$$

where $\Delta\delta_i^e$ and $\Delta\delta_i^p$ are the incremental displacements.

The change in the traction vector across the interface is proportional to the incremental elastic displacement,

$$\Delta T_i = K_i(\Delta\delta_i - \Delta\delta_i^p), \quad (\textit{no summation}) \tag{20}$$

where K_i denote the components of the instantaneous interface stiffness in the x_i-direction.

3.3.1. Damage

From experimental data (Stenberg, 2002b) it was evident that interface damage affects the interface properties. In the model this was accounted for by changing the interface strengths and the interface stiffnesses that are functions of the total effective plastic displacement, δ^p, which is defined as

$$\delta^p = \int_t \Delta\delta^p, \tag{21}$$

where the incremental effective plastic displacement, $\Delta\delta^p$, is defined as

$$\Delta\delta^p = \sqrt{\Delta\delta_i^p \Delta\delta_i^p}. \tag{22}$$

It was assumed that all interface strengths, S_i, decrease as the interface deforms plastically. The strength values decrease according to

$$S_i = S_i^0 e^{-\frac{\delta^p}{\delta_0^s}} + R_i^s, \tag{23}$$

where S_i^0 were the initial interface strengths, R_i^s were the residual strength factors and δ_0^s was a material constant that needs to be determined from experiments.

The interface stiffnesses, K_i, also decrease as the interface deforms plastically,

$$K_i = K_i^0 e^{-\frac{\delta^p}{\delta_0^k}} + R_i^k, \tag{24}$$

where K_i^0 were the initial stiffnesses and R_i^k were the residual stiffness factors and δ_0^k was a material constant that need to be determined from experimental data. Note that the interface strength and stiffness degradation was not equivalent. Residual stiffness R_i^k and strength, R_i^s, factors were used in the model since this improved the stability of the model. When the residual components were used, division with parameters close to zero could be avoided. The residuals were chosen small enough, such that the numbers did not affect the creasing behavior.

Moreover, to prevent the cohesive element from turning inside out during compression the normal stiffness was increased when the displacement in the normal direction (i.e. 1-direction) was less then zero. Hence,

$$K_1 = K_1^0 e^{-10^4 \delta_1} \quad \delta_1 < 0. \tag{25}$$

Plastic interface separation was controlled with a traction based yield surface, $f^{interface}$. Plastic deformation occurred when

$$f^{interface} = \frac{T_1}{S_1} + \frac{T_2^2}{S_2^2} + \frac{T_3^2}{S_3^2} - 1 = 0. \tag{26}$$

It should be noted that when $T_1 = 0$, i.e. for pure shear, an associate flow rule will result in normal dilatation for shear loading. This is a feature that has been observed experimentally by Dunn (2000). The plastic flow rule may be written as

$$\Delta\delta_i^p = \chi\Delta\delta^p \frac{\widehat{M}_i}{\sqrt{\widehat{M}_i \widehat{M}_i}} \tag{27}$$

where M_i were the flow directions and χ indicated if there was plastic deformation, it was defined as

$$\chi = \begin{cases} 1 & \text{if} \quad f = 0 \text{ and } \mathbf{dT} \cdot \frac{\partial f^{interface}}{\partial \mathbf{T}} > 0; \\ 0 & \text{if} \quad f < 0 \text{or} f = 0 \text{ and } \mathbf{dT} \cdot \frac{\partial f^{interface}}{\partial \mathbf{T}} < 0, \end{cases} \tag{28}$$

where $\mathbf{dT} = [dT_1\ dT_2\ dT_3]$. For associated flow the components of the plastic flow direction was expressed as

$$\widehat{M}_1 = \frac{\partial f}{\partial T_1} = \frac{1}{S_1} \tag{29}$$

$$\widehat{M}_i = \frac{\partial f}{\partial T_\alpha} = 2\frac{T_\alpha}{S_\alpha^2} \quad i = 2, 3 \tag{30}$$

3.4. Implementation

Both the continuum and cohesive models have been implemented as a user-defined material (UMAT) in ABAQUS (2008).

The system of equations needed, to solve the elastic–plastic problem, was formulated using a radial return algorithm. When an element deformed plastically the Newton–Raphson method was used to solve the system of equations. In the solution scheme all variables were defined in the new time step. In addition the material Jacobian for the continuum model, $\partial\sigma/\partial\varepsilon$, and for the cohesive model, $\partial T/\partial\delta$, were provided to ABAQUS (2008) in each time step.

3.5. Interactions

Between the paperboard model and both the female die and the male die interactions were defined. The interaction properties define both the normal and tangential behaviors. In the normal direction an exponential overclosure behavior was used (ABAQUS, 2008). Both for the male die and the female die the contact pressure was $p_0 = 0.5$ MPa and clearance for the male die was $c_0^{male} = 10^{-3}$ mm, while it was $c_0^{female} = 10^{-4}$ mm for the female die. Other contact models were tested, but the exponential overclosure model worked best for this model. In the tangential direction a Coulomb friction model (ABAQUS, 2008) with coefficient 0.7 was used for the interaction between the paperboard and female die. For the male die no tangential behavior was defined.

3.6. Boundary conditions

For all simulations the male die was moved from its initial position above the paperboard down to either position $z = 0.00$ mm or $z = 0.20$ mm. Webtension was applied by a displacement in the x-direction, which were chosen in order to give the same initial force in the in-plane directions as the ones measured in the experiments.

4. Results

In this work a commercial paperboard was used, which was seen in Fig. 1. The paperboard had three plies, where the outer plies were denser than the middle ply, and also the fiber composition and processing differed between the middle and outer plies. The positions of the interfaces between the two outer plies and the middle ply were determined by grinding. In the model generation, the geometry was partitioned along the interfaces before meshing. The meshing was thereafter made such that at least two continuum element rows were used to represent each ply in the thickness direction. In Fig. 5 the different plies and interfaces are seen. To incorporate the cohesive elements an orphan mesh (ABAQUS, 2008) was created to enable the insertion of cohesive elements with initial thickness zero. In the model, cohesive elements were inserted between the plies. However, in order to improve the numerical performance, the elements were inserted only in the creasing area, as seen in Fig. 5.

To shorten the computational time, and also to improve numerical reliability, the model was only 0.1 mm long in the CD direction, while in the experimental setup the specimens were 38 mm wide. Instead a plane strain condition was used in the CD direction. In the proposed model the number of elements could be kept low and well shaped.

4.1. Determination of material parameters

The paperboard as well as its plies and interfaces have been characterized with respect to elastic–plastic properties, where the two outer and the middle plies were characterized independently. The characterization methods which have been described by Nygårds (2008) were used, and included: in-plane tension, cyclic ZD tension, cyclic ZD compression and out-of-plane shear. The determined material data are found in Appendix A in Tables A.1–A.3.

In the experimental characterization of the plies it was difficult to measure out-of-plane continuum shear properties. In experimental shear tests paperboard has a tendency of delamination. Hence, continuum shear properties can not be determined. In the theoretical model shear hardening was expressed in Eq. (17), where the τ_0, A_τ and B_τ were material constants. However, here τ_0 was taken as the experimentally measured shear peak load, while the values of A_τ and B_τ were chosen to fit the experimental creasing curves.

4.2. Creasing of paperboard

In Fig. 6, the numerical and experimental data for simulations with female die width $w_{female} = 1.6$ mm and male die width $w_{male} = 0.9$ mm have been plotted for creases down to displacements 0.00 and 0.20 mm. At zero displacement the male die was at the female die level. In Fig. 6, it was observed that the loading part of the creasing curve was well captured for crease depth 0.00 mm. During unloading, the experimental data initially were stiffer, as seen in Fig. 6, which also resulted in bad predictions of the residual indent, which was −0.26 mm in the experiments and −0.22 mm in the simulation. It was believed that this was due to the geometrical description and the friction between the paperboard and the female die.

When the crease depth was increased to 0.20 mm, the experimental data and the numerical model showed a hardening effect during loading when the displacement exceeded 0.0 mm, which is seen in Fig. 6. In the numerical model this was controlled by the B_τ parameter, a larger value will result in a greater hardening effect, which also was captured well in the simulations. As seen in Fig. 6, there was a small deviation between the simulation and experimental data at peak load. This was due to initiated delamination in the cohesive elements. In the numerical model the cohesive elements were discretized and had fixed positions, while in the real paperboard the interfaces were rough. Therefore, delamination could more easily be initialized in the numerical model. During unloading the experimental results were well predicted by the simulation.

In Fig. 7, the evolution of the in-plane force as function of male die displacement is shown. During initial unloading from male die displacement 0.20 mm the simulations did not capture the exper-

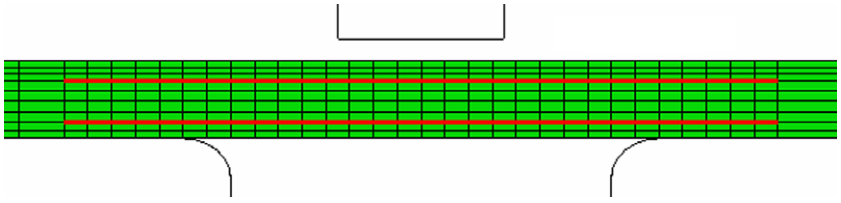

Fig. 5. Mesh used in the creasing area. In the figure the cohesive elements have been colored red, those are positioned in the creasing area. The paperboard has two interfaces. Above the cohesive elements the top ply was located, and below the cohesive element the bottom ply can be seen.

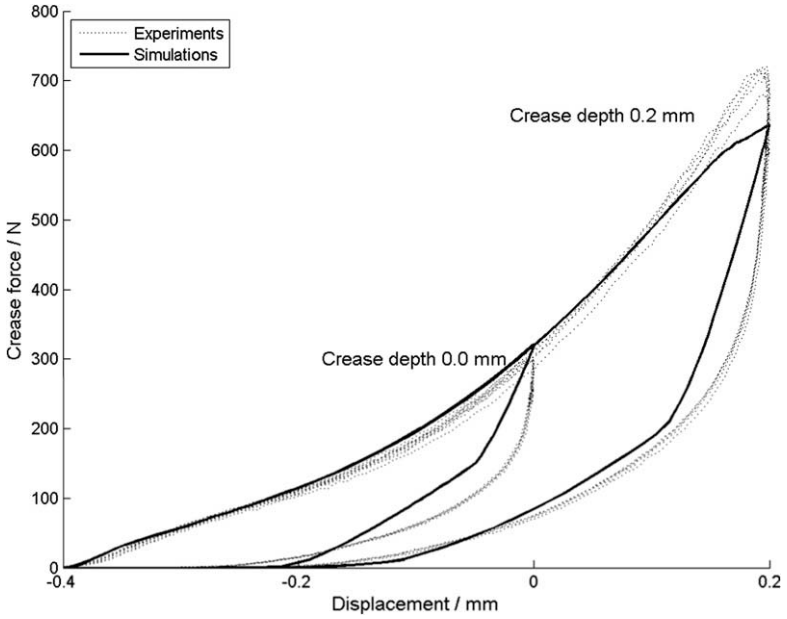

Fig. 6. Comparison between experimental data and simulations for crease depths 0.00 and 0.20 mm.

imental curves very well, which probably was due the initiation of delamination in the simulations. Apart from that the simulations predict the experimental behavior well.

In Figs. 8 and 9 contour plots for creasing depths 0.00 and 0.20 mm are shown. In Fig. 8ab and Fig. 9ab it can be observed that the maximum ZD compression strains, ε_{zz}, became 32% and 44%, which corresponded to ZD compressive stresses, σ_{zz}, of 6 and 11 MPa, respectively. Moreover, the creasing operation generates a quite uniform shear strain, γ_{xz}, field, as seen in Fig. 8c and 9c. In fact the creasing operation, with the measured material constants, seems to be an excellent shear test. When the paperboard had been unloaded it was observed that large amount of plastic ZD strain, ε_{zz}^{p}, and plastic shear strain, γ^{p}, were present in the continuum elements in the creasing area, as seen in Figs. 10ab and 11ab. Hence, although the cohesive elements took a great deal of the out-of-plane deformations, since delamination was initiated; the plastic models used in the continuum elements contribute much to the overall behavior. In Fig. 11c, after creasing to crease depth 0.2 mm, it was observed that a small amount of plastic in-plane strain had developed, however this was only observed in the middle ply. This could not be detected in Fig. 10c, where the model had been creased to depth 0.0 mm. In Fig. 11 the opening of the cohesive elements can also be observed. Especially the top interface opens up, which is due to elastic energy release that depends on the elastic properties of the paperboard.

In the creasing operation it is important to damage the paperboard enough to enable subsequent forming. One of the reasons to produce multiply paperboards is to simplify permanent deformation of the paperboard through delamination between the plies. With the developed material and finite element models,

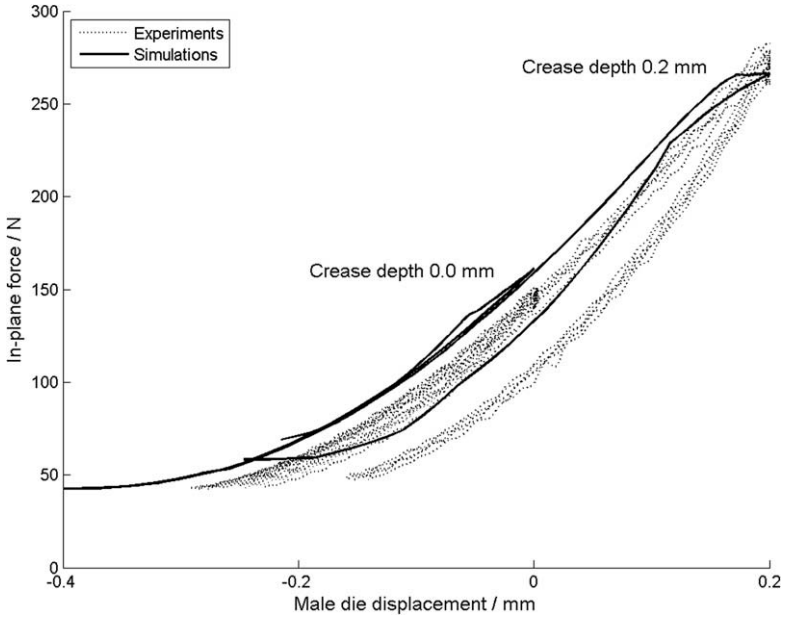

Fig. 7. Comparison between experimental data and simulations of web tension for crease depths 0.00 and 0.20 mm.

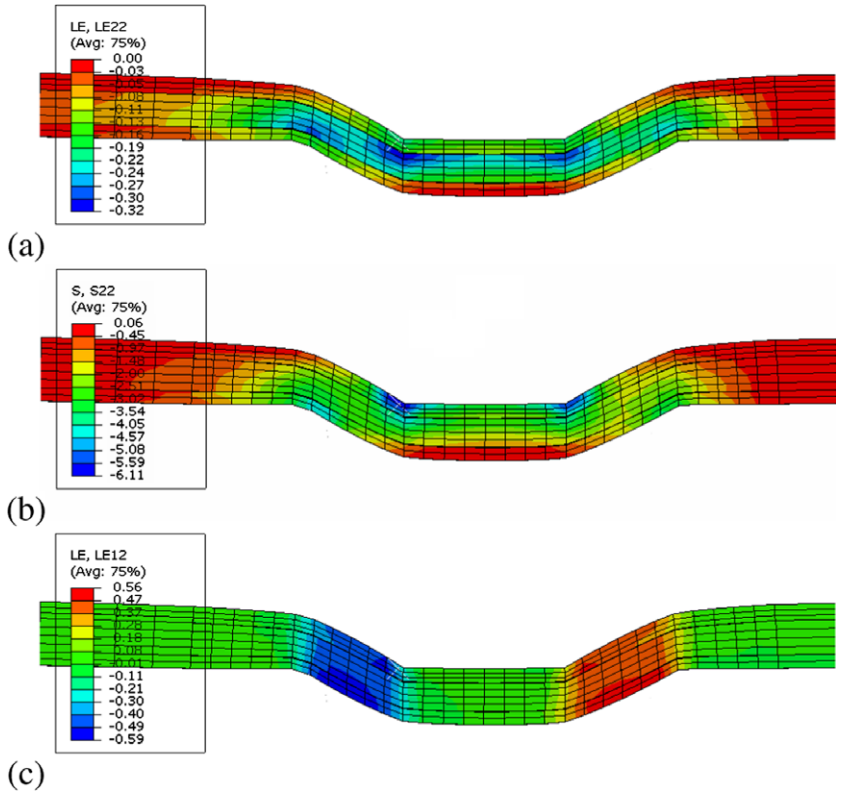

Fig. 8. Contour plots for creasing depth 0.0 mm. (a) Strain in ZD direction (ε_{zz}) and (b) stress in ZD direction (σ_{zz}) (c) shear strain γ_{xz}.

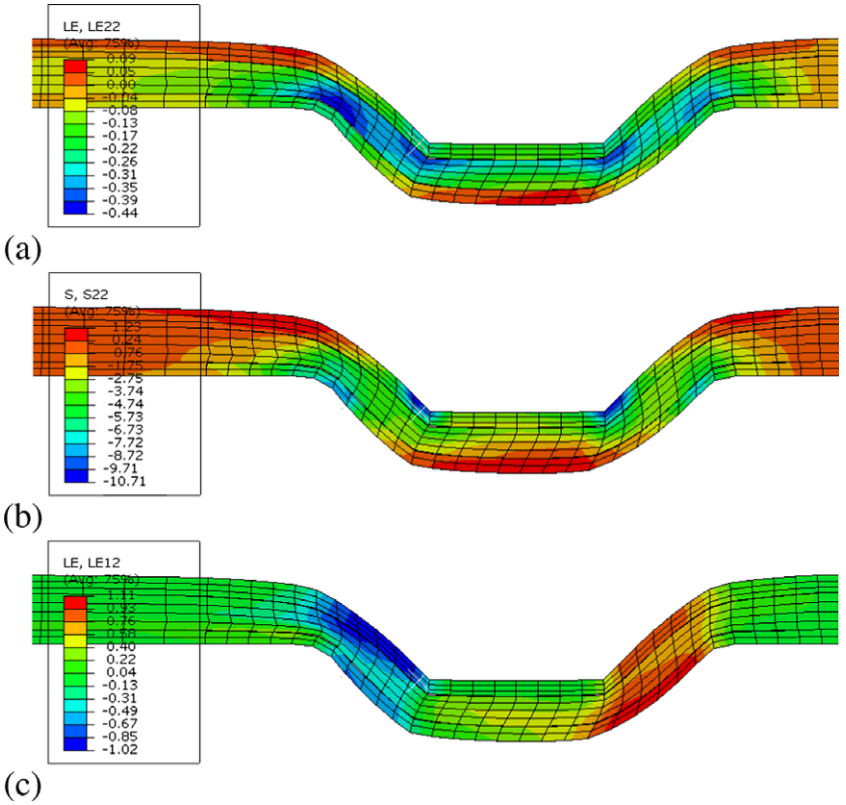

Fig. 9. Contour plots for creasing depth 0.2 mm. (a) Strain in ZD direction (ε_{zz}) and (b) stress in ZD direction (σ_{zz}) (c) shear strain γ_{xz}.

studies of damage evolution along the interfaces have been enabled. In Fig. 12, the effective plastic displacement, δ^p, has been plotted for the top and bottom interfaces at the peak load and after unloading. In Fig. 12, it can be seen that the effective plas-

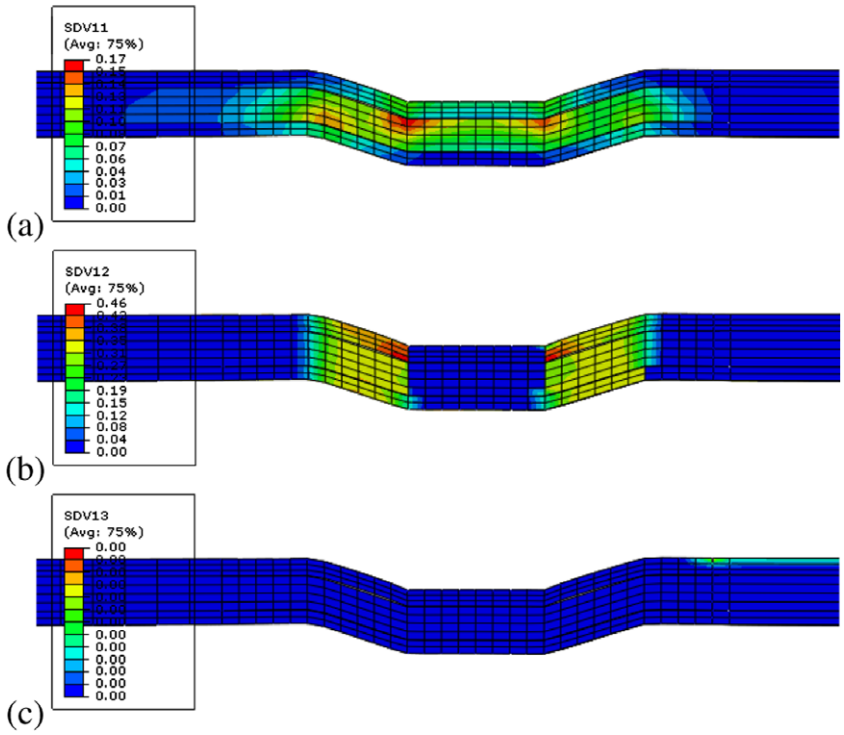

Fig. 10. Plastic strain components after unloading from creasing depth 0.00 mm. (a) plastic ZD strain (ε_{zz}^{p}) (b) plastic shear strain (γ^{p}) (c) plastic in-plane strain (ε_{eff}^{p}).

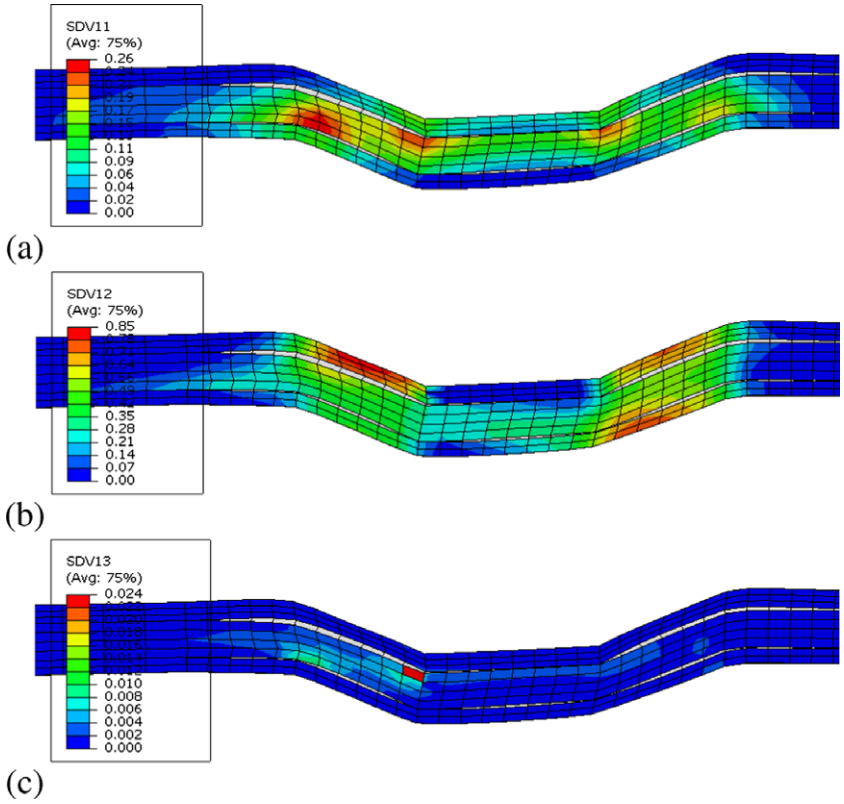

Fig. 11. Plastic strain components after unloading from creasing depth 0.20 mm. (a) plastic ZD strain (ε_{zz}^{p}) (b) plastic shear strain (γ^{p}) (c) plastic in-plane strain (ε_{eff}^{p}).

tic displacement have evolved in the top interface already at peak load, but only in the region between the male and female dies. In the bottom interface no plastic displacement was observed. After unloading interface opening was observed. However, there was a considerable difference between the two male die loading depths, 0.00 and 0.20 mm. In the latter case, the plastic displacement was much larger in both interfaces, and damage was observed outside the female die. For both inter-

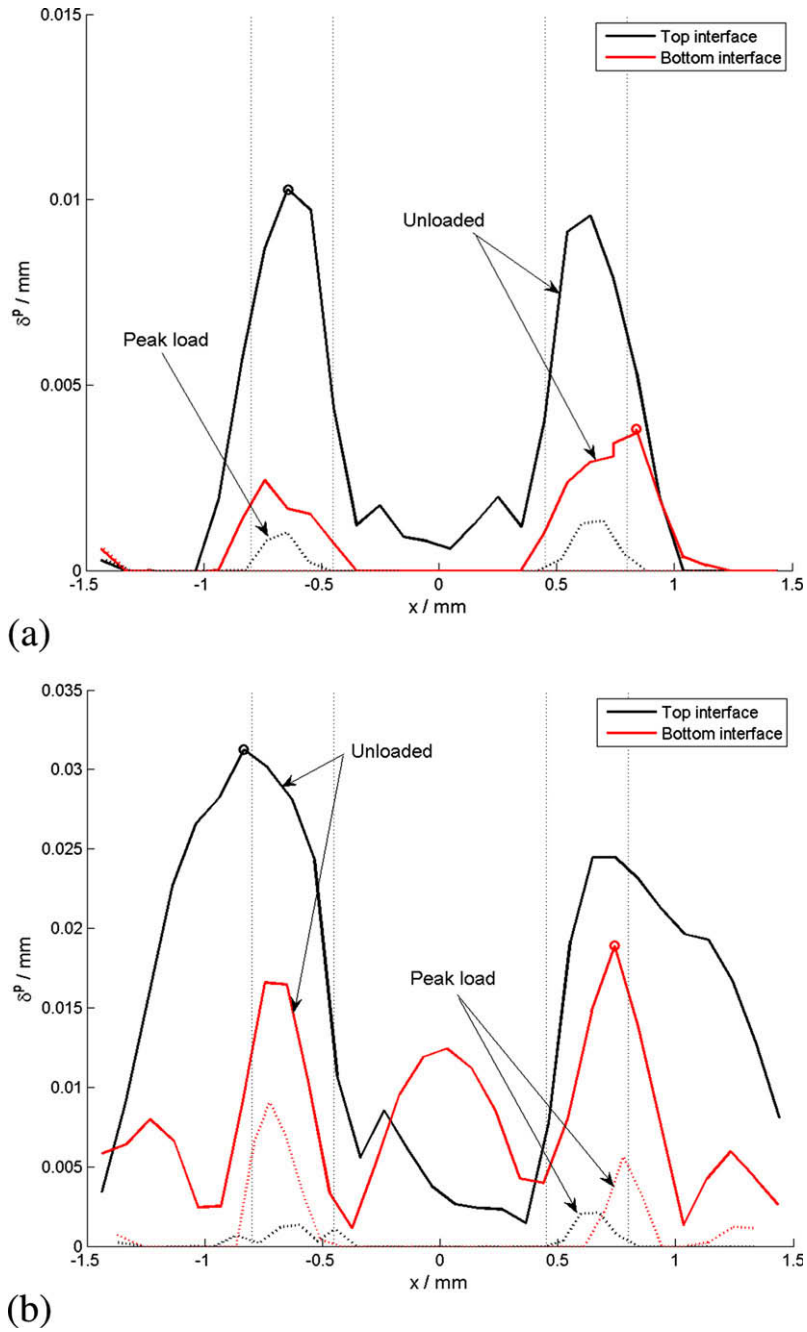

Fig. 12. Effective plastic displacement in the top and bottom interfaces for (a) crease depth 0.00 mm and (b) crease depth 0.20 mm. Solid lines in the plot represent the plastic displacement along the interface after unloading, while dashed lines represent the peak load. the vertical lines indicates the positions of the male and female dies. The circles indicate the elements with maximum damage after unloading along each interface; these elements have been chosen to generate Fig. 13.

faces and loading depths, the plastic displacement beneath the male die was fairly small.

In Fig. 12 the elements with maximum damage after unloading in each interface have been indicated by circles. The effective plastic displacement evolution as function of male die displacement for these elements has been evaluated in Fig. 13. For the top interface it was observed that the cohesive elements start to deform plastically when the male die displacement was about −0.3 mm, i.e. when the male die had been pushed 0.1 mm into the paperboard. Thereafter the effective plastic displacement accumulated, and saturated when the male die displacement became 0.0 mm. At this point the paperboard was pushed into the female die, which compressed the paperboard and prevented interface separation. Upon unloading the paperboard was elastically unloaded both in tension and shear, hence the both interfaces started to open up. For all elements in Fig. 13, the major part of the effective plastic displacement build-up took place when the male die had returned to about −0.2 mm. For both crease depths the plastic displacement build-up saturated at male die displacement −0.2 mm. In Fig. 13b it can be observed that the bottom interface at crease depth 0.2 mm had the greatest damage at the peak load. When the male die displacement exceeded 0.1 mm the bottom interface element in Fig. 13b deformed due to shear deformation. Upon unloading the elastic shear deformation was released in the interval around male die displacement 0.1 mm. Thereafter the damage level reached a constant plastic displacement which was maintained until the male die displacement became −0.06 mm, where the element started to open up in its normal direction.

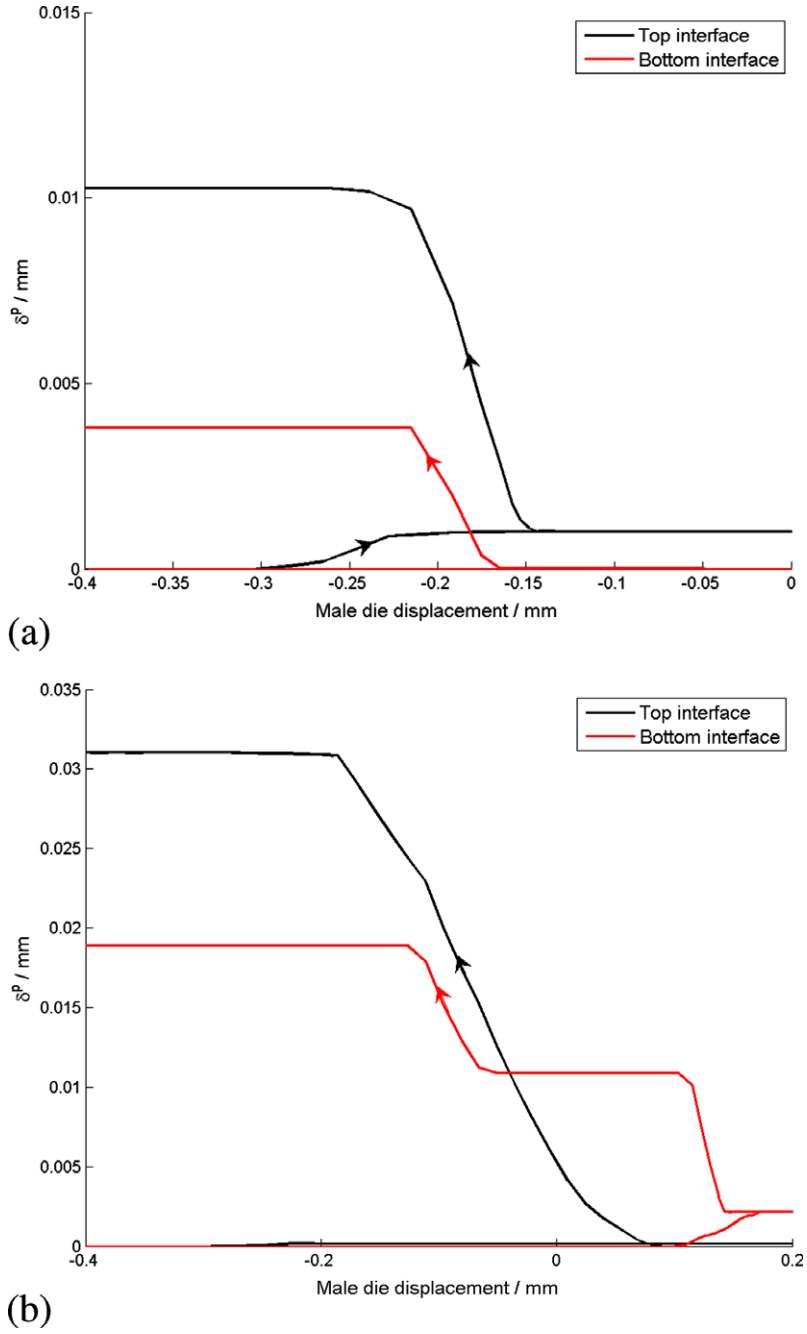

Fig. 13. Evolution of plastic displacement as function of male die displacement in the elements with maximum damage, which were indicated in Fig. 12, for (a) crease depth 0.0 mm and (b) crease depth 0.2 mm.

5. Discussion and conclusions

Based on experiences with the creasing models, the importance of different parameters has been identified. The shear properties dominate the loading part of the force–displacement curve. However, at zero displacement, the male die has reached the level of the female die. Then the compression in the thickness direction of the paperboard becomes important, whereby the curve shows a stiffer response. Initially upon unloading, the friction between the paperboard and the tools dominate the unloading response. Thereafter the paperboard was elastically decompressed.

The main purpose of the creasing operation is to introduce damage in the paperboard to locally reduce its bending stiffness. During loading it therefore important that the paperboard easily delaminates between its plies since this reduces the bending stiffness during folding. Moreover, the plies should internally be able to deform plastically in shear. By considering the microstructure of paperboard, these requirements are met if the paperboard has well defined plies with weak interfaces. Moreover, within the plies the shear stresses should ideally break bonds but not the fibers. This would enable plastic shear deformations with maintained elastic stiffnesses. In the analysis it was showed that the main part of interface opening occurred during decompression of the paperboard. In order to maximize the opening it is important that the elastic stiffnesses are maintained during loading, i.e. if primarily bonds and not fibers have been broken. Finally, it was observed that higher friction between the tools and paperboard contribute to interface opening in the paperboard.

Material models that predicts mechanical behavior of paperboard has been and still is active research. For most other materials, such as metals, plastics and ceramics etc, the constitutive behavior is well known. Therefore, material models exist in every commercial finite element program. When a three dimensional model for paperboard is desired, i.e, when the thickness direction is incorporated, the constitutive behavior needs to be divided into a continuum and an interface behavior, which has been presented here. With this approach it was possible to capture the essence of the paperboard deformation and damage mechanisms. Finally it can be concluded that with the proposed material model it will be possible to perform finite element simulations that can be used to investigate different types of material behavior. The effect of different material properties can e.g. be investigated virtually before any paperboard have been manufactured. This can potentially shorten the development process of new paperboard grades. If different types of loadings and material behaviors are investigated with simulations, this knowledge can be used to design paperboard with respect to interface and ply properties in the thickness direction. With the simulations, it then becomes possible to identify and develop know-how about important damage and deformation mechanisms in the converting process. Hence properties that are important for the manufacturer, which can be linked to properties that are important for the end-user.

Acknowledgement

The development of the numerical models in this work has been financed by the Liquid Paperboard cluster at STFI-Packforsk. While the development of the creasing equipment has been financed by Tetra Pak.

Appendix A. Material properties

See Tables A.1–A.3

Table A.1
Material properties for the bottom, middle and top plies.

Notation	Bottom	Middle	Top
Elastic in-plane parameters			
E_1/MPa	7122.32	4029.20	7361.53
E_3/MPa	2948.39	1823.55	2788.49
ν_{13}	0.46	0.44	0.48
G_{13}/MPa	1685.69	1023.02	1764.07
Yield surface and hardening			
σ^{I}_{s0}/MPa	39.13	25.58	41.57
σ^{II}_{s0}/MPa	17.23	10.93	17.41
σ^{III}_{s0}/MPa	24.64	16.48	24.54
σ^{IV}_{s0}/MPa	39.13	25.58	41.57
σ^{V}_{s0}/MPa	17.23	10.93	17.41
A^{I}/MPa	13.60	6.12	10.10
A^{II}/MPa	6.54	4.02	9.10
A^{III}/MPa	5.82	11.66	6.38
A^{IV}/MPa	13.60	6.12	10.10
A^{V}/MPa	6.54	4.02	9.10
B^{I}	225.15	224.89	206.46
B^{II}	150.62	140.50	117.54
B^{III}	117.25	37.68	144.25
B^{IV}	225.15	224.89	206.46
B^{V}	150.62	140.50	117.54
C^{I}/MPa	2005.80	891.60	1615.39
C^{II}/MPa	473.23	209.73	242.94
C^{III}/MPa	865.05	253.82	552.02
C^{IV}/MPa	2005.80	891.60	1615.39
C^{V}/MPa	473.23	209.73	242.94
$2k$	4.00	4.00	4.00
Biaxial deformation			
$d\varepsilon^{p}_{CD}/d\varepsilon^{p}_{MD}$	−0.46	−0.44	−0.48
$d\varepsilon^{p}_{MD}/d\varepsilon^{p}_{CD}$	−0.19	−0.20	−0.18

Table A.2
Out-of-plane continuum material properties for the bottom, middle and top plies.

Notation	Bottom	Middle	Top
Out-of-plane normal model			
E_2	14.00	13.00	20.00
E_c	0.47	0.38	0.47
C_c	24.46	16.33	24.46
A_p	16.55	11.88	16.55
B_p	3.16	1.92	3.16
Out-of-plane shear model			
G_{12}	30.0	35.0	84.0
τ_0	2.1	0.95	2.7
A_τ	9.0	9.0	9.0
B_τ	2.0	2.0	2.0

Table A.3
The cohesive material properties for the interfaces.

Notation	Interface
K^0_{MD}	925.00
K^0_{ZD}	360.00
S^0_{MD}	1.22
S^0_{ZD}	0.24
K^0_{CD}	880.00
S^0_{CD}	1.03
δ^s_0	0.18
R^s_{ZD}	0.05
R^s_{MD}	0.01
R^s_{CD}	0.00
δ^k_0	0.00
R^k_{ZD}	1.00
R^k_{MD}	1.00
R^k_{CD}	1.00

Appendix B. Supplementary data

Supplementary data associated with this article can be found, in the online version, at doi:10.1016/j.ijsolstr.2009.02.014.

References

ABAQUS, 2008. ABAQUS User's Manual, 6.8 ed. Abaqus Inc., Providence, RI, USA..
Andersson, T., 2006. A small deformation model for the elasto-plastic behavior of paper and paperboard. Master's Thesis, Lund University..
Ask, A., 2007. Simulation model for anisotropic fibrous materials. Master's Thesis, Division of Solid Mechanics, Lund Univesity..
Baum, G.A., Brennan, D.C., Haberger, C.C., 1981. Orthotropic elastic constants of paper. TAPPI 64 (8), 97–101.
Carlsson, L., Feller, C., Westerlind, B., 1982. Finite element analysis of the creasing and bending of paper. Svensk Papperstidning 85 (15), 121–125.
Carlsson, L., Ruvo, A.D., Fellers, C., 1983. Bending properties of creased zones of paperboard related to interlaminare defects. Journal of Materials Science 18, 1365–1373.
Cavlin, S., 1988. The unique convertibility of paperboard. Packaging Technology and Science 1, 77–92.
Cavlin, S., Dunder, I., Edholm, B., 1997. Creasability testing by inclined rules – a base for standardized specification of paperboard. Packaging Technology and Science 10, 191–207.
deRuvo, A., Carlsson, L., Fellers, C., 1980. The biaxial strength of paper. TAPPI 63, 133–136.
Dunn, H.M., 2000. Micromechanics of paperboard deformation. Master's Thesis, Massachusetts Institute of Technology..
Hallbäck, N., Girlanda, O., Tryding, J., 2006. Finite element analysis of ink-tack delamination of paperboard. International Journal of Solids and Structures 43, 899–912.
Harrysson, A., 2007. Anisotropy at finite strains and application to paper materials. Licentiate Thesis, Solid Mechanics, Lund University..
Hine, D.J., 1987. The rigidity/flexability balance in the creasing of paper based boards. Appita 40, 375–378.

Mäkelä, P., Östlund, S., 2003. Othotropic elastic–plastic material model for paper materials. International Journal of Solids and Structures 40 (21), 5599–5620.
Nagasawa, S., Fukuzawa, Y., Yamaguchi, T., Tsukatani, S., Katayama, I., 2003. Effect of crease depth and crease deviation on folding deformation characteristics of coated paperboard. Journal of Material Process Technology 140, 157–162.
Nagasawa, S., Endo, R., Fukuzawa, Y., Uchino, S., Katayama, I., 2008. Creasing characteristic of aluminum foil coated paperboard. Journal of Material Process Technology 140, 157–162.
Nygårds, M., 2008. Experimental techniques for characterization of elastic–plastic material properties in paperboard. Nordic Pulp and Paper Research Journal 23 (4), 432–437.
Nygårds, M., Hallbäck, N., Just, M., Tryding, J., 2005. A finite element model for simulations of creasing and folding of paperboard. In: ABAQUS Users's Conference 2005..
Öhrn, O.E., 1965. Thickness variations of paper on stretching. Svensk Papperstidning 68 (5), 141–149.
Stenberg, N., 2002a. On the out-of-plane mechanical behavior of paper materials. PhD Thesis, Royal Institute of Technology (KTH), Solid Mechanics..
Stenberg, N., 2002b. Out-of-plane shear of paperboard under high compressive loads. Journal of Pulp and Paper and Paper Science 30 (1), 22–28.
Stenberg, N., Fellers, C., 2002. The out-of-plane Poisson's ratios of paper and paperboard. Nordic Pulp and Paper Research Journal 17 (4), 387–394.
Tryding, J., 1996. In-plane fracture of paper. PhD thesis, Lund Institute of Technology, Division of Structural Mechanics..
Xia, Q., Boyce, M., Parks, D., 2002. A constitutive model for the anisotropic elastic–plastic deformation of paper and paperboard. International Journal of Solids and Structures 39, 4053–4071.
Xia, Q.S., 2002. Mechanics of inelastic deformation and delamination in paperboard. PhD thesis, Massachusetts Institute of Technology..